CHAPTER 2

Effect of Heat Treatment on the Colloidal ZnO QDs Based Charge Transport Layer on the Performance Characteristics of ZnO QDs/CdSe QDs/MoO_x/Ag Thin Film Photodetectors*

Contents

2.1 Introduction 39

2.2 Experimental Details 40

2.2.1 Preparation of Colloidal ZnO QDs 41

2.2.2 Preparation of Colloidal CdSe QDs 42

2.2.3 Device Fabrication 44

2.3 Result and Discussion 44

2.3.1 Structural characterization of as-grown ZnO QD and CdSe QD 44

2.3.2 Device Characterization 46

2.3.3 Suitability of Annealed Colloidal ZnO QDs for Thin Film Transistors 57

2.4 Conclusion 61

*Part of this work has been published as:

Hemant Kumar et al. "Heating Effects of Colloidal ZnO Quantum Dots (QDs) on ZnO QDs/CdSe QDs/MoO_x Photodetectors," *IEEE Transactions on Nanotechnology*, 16(6):1073-1080, 2017.

Hemant Kumar et al. "Kink Effect in TiO_2 Embedded ZnO Quantum Dot based Thin Film Transistors," *Electronics Letters*, 53(4):15–16, 2017.

CHAPTER 2

Effect of Heat Treatment on the Colloidal ZnO QDs Based Charge Transport Layer on the Performance Characteristics of ZnO QDs/CdSe QDs/MoO_x/Ag Thin Film Photodetectors

2.1 Introduction

The leakage current or dark current in the photodetectors (PDs) is always undesirable since it deteriorates the performance of the detectors (Baeg et al. 2013). It has been observed from the literature survey in Chapter-1 that the dark current in the PDs depends on the proper selection of electrodes (Xue & Forrest 2004), semiconductor-metal interfaces (Agostinelli et al. 2008), inter-electrode spacing (Ng et al. 2008; Ramuz et al. 2008), and selection of proper charge transport layers (Yu et al. 2013) in the device. The proper selection of charge transport layers can improve the performance of the PDs by optimizing the charge trapping states and roughness of the active layers (Drndić et al. 2002; Yu et al. 2013; Lattante 2014). It has been discussed that ZnO QDs can be used as a good electron transport layer in the CdSe QDs based PDs due to its large band gap energy (~ 3.37 eV) and high exciton energy (~ 60 meV). Since the annealing temperature affects the absorption spectrum and crystallite size of the ZnO NPs (Kumar et al. 2017; Drndić et al. 2002; Raoufi & Raoufi 2009), we have investigated the effects of heat treatment of the colloidal ZnO QDs based ETL on the performance of ZnO QDs/CdSe QDs/MoO_x/Ag based PDs where the colloidal CdSe QDs layer has been used to act as the active layer in the device. The proposed PDs under consideration have been fabricated by the low-cost solution processed spin coating technique. The performance of the PD under study has been investigated

corresponding to the annealing of the ZnO QDs ETL at three different temperatures of 250°C, 350°C, and 450°C in the ambient environment. The outline of the rest of the chapter is given as follows.

Section 2.2 is devoted to describing the fabrication details of the PDs under study. The results and related discussions regarding the film morphology and current-voltage characteristics under dark and illuminated conditions of the PD have been discussed in Section 2.3. The suitability of the annealed ZnO QDs at high temperature for other electronic devices such as the thin film transistors (TFTs) has also been discussed in this section. Finally, Section 2.4 has been used to summarise and conclude the works presented in the chapter.

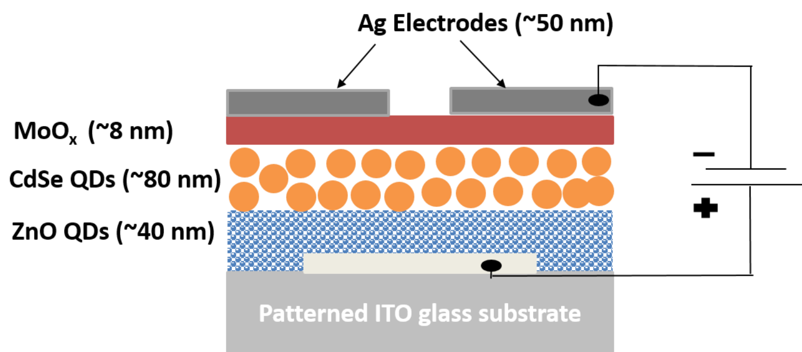

Figure 2.1: Complete device schematic with Ag (~50 nm)/MoO_x (~8 nm)/CdSe QDs (~80 nm)/ZnO QDs (~40 nm)/ITO

2.2 Experimental Details

We have fabricated the ITO/ZnO QD/ CdSe QD/ MoO_x/Ag structure based photodetectors on the cleaned patterned ITO substrates using solution processed spin coating technique as shown in Figure 2.1. Three types of photodiodes namely A, B, and C have been considered containing the ZnO QDs layer annealed at three different temperatures 250°C, 350°C and 450°C, respectively. For device fabrication, initially the substrates were cleaned thoroughly using alcanox, deionized (DI) water, acetone, and

isopropanol sequentially and then dried at 90°C for 15 mins. All the chemicals used in the cleaning process were from the MERCK-Chemical Limited, Mumbai, India. The synthesis of monodisperse colloidal QDs (with the standard deviation in size < 8%) is achieved by maintaining the constant temperature while injection and after the injection to obtain a uniform colloidal QDs (Klimov 2010). Since temperature plays an important role in the preparation of monodisperse colloidal QDs, a suitable temperature (e.g., 60°C for ZnO and 140°C for CdSe) is maintained at the injection to start the nucleation of QDs (Klimov 2010). Further, a short nucleation of QDs with a slow growth rate is maintained to achieve monodisperse colloidal QDs (Murray et al. 2001) as a function of temperature and the concentration of monomer. It may be mentioned that the growth of particle is enhanced when the monomer concentration is maintained well below the critical concentration for nucleation (Murray et al. 2001).

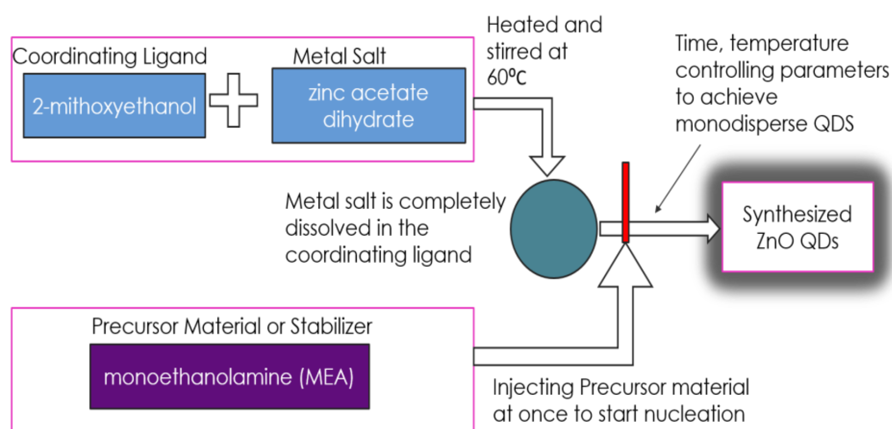

Figure 2.2: Flowchart of ZnO QD synthesis under the inert environment.

2.2.1 Preparation of Colloidal ZnO QDs

The preparation of colloidal ZnO QDs is performed using Zinc acetate dihydrate ($Zn(CH_3COO)_2.2H_2O$) as a precursor material without any further purification. The precursor material is dissolved in the 2-methoxyethanol used as the coordinating ligand and followed the method as described in (Kumar et al. 2017). The solution is further

stirred for 24 hrs in an inert atmosphere and then filtered using PVDF membrane (0.22 μm) to filter out the un-reacted and large size particles from the solution for enhancing the surface uniformity. The detailed flow chart of ZnO QD synthesis is shown in Figure 2.2. The ZnO QDs are uniformly dispersed in the solution of 2-methoxyethanol and MEA, the boiling point of monoethanolamine (MEA) is ~170-190°C. This boiling point of MEA introduces the lower limit of annealing for ZnO QDs prepared using this method. The prepared solution of the colloidal ZnO QDs was finally deposited by spin coating (SPM-150LC, GmbH) method on patterned ITO substrates (15 x 15 mm^2). The speed of spin coater is maintained at 3000 rpm for 2 mins and then the ZnO QD coated samples are dried under the ambient environment at 150°C. The process was repeated to achieve the desired thickness of ~40 nm measured using Reflectometer (F-20, Filmetrics). Annealing of the ZnO QDs performed under the ambient environment at 250°C, 350°C, and 450°C and the respective devices were labeled as A, B, and C, respectively.

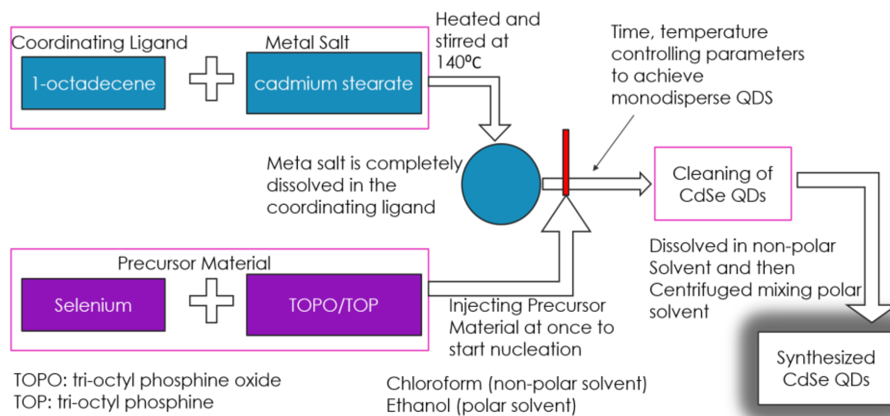

Figure 2.3: Flowchart of CdSe QD synthesis under the inert environment.

2.2.2 Preparation of Colloidal CdSe QDs

The high-quality nanocrystal QDs of CdSe is synthesized by using colloidal nano synthesis method (Murray et al. 2000). This process can be divided into multiple

processes starting from the nucleation by injecting precursor material at a suitable temperature. This phenomenon leads to the growth of particles from the solution and simultaneously starts Ostwald ripening (recrystallization or aging). It is hugely dependent on the presence of strong coordinating ligands which may alter nucleation and growth process (Murray et al. 2000; Klimov 2010). Here, octadecene has been used as a coordinating ligand, cadmium stearate as a metal salt and selenium powder mixed with TOPO (tri-octyl phosphine oxide) are used as the precursor material. The precursor material is injected in the coordinating ligand with the metal salt at 140°C to start nucleation, and the reaction is quenched after two minutes to attain the required size of CdSe QDs. Further, the moderately heated solution of CdSe QDs with toluene and ethanol are centrifuged at 5000 rpm for 10 mins. Due to the effect of centrifugal force, the CdSe QDs particle precipitate and the remaining solution is discarded consisting of unwanted and unreacted materials. The precipitated CdSe QDs are dried under the ambient environment and then dissolved in chloroform (10 mg/ml) to achieve a uniformly dispersed solution of colloidal CdSe QDs. The detailed flow chart of CdSe QD synthesis is shown in Figure 2.3. The prepared solution of CdSe QDs (~80 nm) is deposited over the annealed ZnO QDs /patterned ITO substrates using spin coating (SPM-150LC, GmbH) at 1500 rpm for 2 mins and then heated at 80°C to obliterate the chloroform solution from the device. The CdSe QDs layer is then coated with the ethanedithiol for introducing the Mid-Gap Band (MGB) to improve the conductance of the QDs (Pal et al. 2012). Note that the surface treatment by ethanedithiol does not affect the size of the CdSe QDs but modifies the surface properties of the CdSe QDs through the passivation ligands (Pal et al. 2012; Tang et al. 2011).

2.2.3 Device Fabrication

A thin MoO_x layer (~8 nm) is deposited on the CdSe QDs to act as the hole transport layer (HTL) (Litzov & Brabec 2013). A high purity (99.99%) Ag layer (~50 nm) is then deposited on the MoO_x layer in rectangular form as a contact electrode. In addition to acting as the HTL, the MoO_x layer also improves the electrode work function of the device equivalent to the Au electrodes (Brown et al. 2011). Both the MoO_x and Ag layers are grown by thermal deposition method (HHV, FL400 SMART COAT 3.0 A) on the sol-gel derived CdSe QDs using the shadow mask technique for a contact area of 0.075 cm^2 (effective area of Ag contact pad). Thermal deposition of evaporating materials is performed at high vacuum (~10^{-6} mbar) at the rate of 1.00 Å/s by maintaining the separation between source and substrate as ~18 cm.

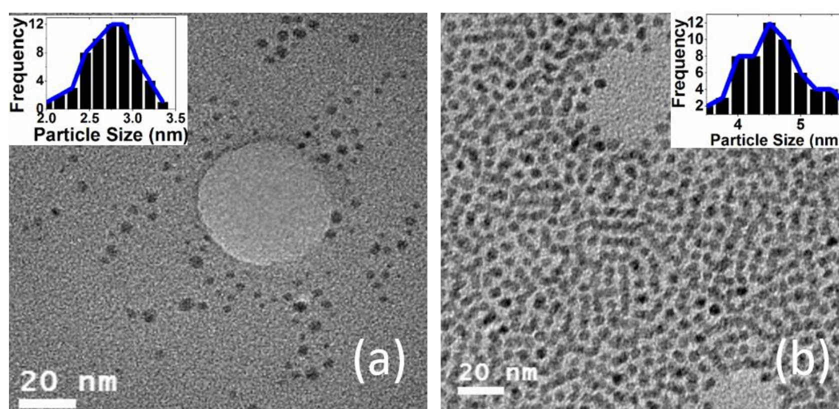

Figure 2.4: (a) TEM image of as-grown ZnO QDs with particle size histogram and (b) TEM image of as-grown CdSe QD with particle size histogram**.**

2.3 Result and Discussion

2.3.1 Structural characterization of as-grown ZnO QD and CdSe QD

The transmission electron microscopy (TEM) image from TECNAI G2 20 TWIN of the as-grown ZnO QDs and CdSe QDs is shown in Figure 2.4 (a) & (b). The histogram plot of both ZnO and CdSe QDs are shown in the inset of Figure 2.4 (a) &

(b). The histogram (particle size against no. of particles) of CdSe QDs indicates the mean particle size of ~4.58 nm with a standard deviation of 0.58 nm and for ZnO QDs the mean particle size obtained is ~2.31 nm with a standard deviation of 0.35 nm. The obtained particle size is less than the respective Bohr's radius of CdSe (~5.6 nm) and ZnO (~2.87 nm) QDs.

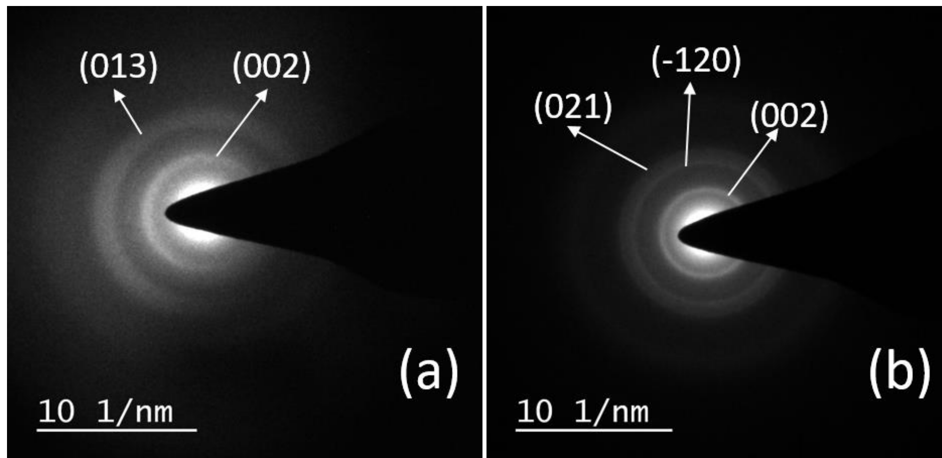

Figure 2.5: Selected area electron diffraction pattern of (a) as-grown ZnO QD and (b) as-grown CdSe QD.

The selected area electron diffraction pattern (SAED) pattern of the multiple particles show the continuous diffused concentric rings shown in Figure 2.5 (a) & (b) indicates particle size are indeed small, which cannot hold more than one grain. This constraint is due to the large surface to volume ratio of QDs and hence assumes the single crystallinity of the particle. The orientation of these particles can be found by the analysis of rings present in SAED pattern. For the ZnO QDs, the rings are indexed to <002> and <013> with a d-spacing of 2.66 Å and 1.48 Å, respectively using a Crystallography Open Database (COD) number 2300112 (Sowa & Ahsbahs 2006). Further, the orientation of CdSe particles are found to be <002>, <-120>, and <021> with a d-spacing of 3.55 Å, 2.14 Å, and 1.78 Å, respectively using a COD number 9016056 (Freeman et al. 1977). Cell structure for both CdSe and ZnO QDs confirms to

be hexagonal (wurtzite) structure with a lattice parameter of a=4.299 Å, c=7.0100 Å for CdSe (Freeman et al. 1977) and a=3.2494(2) Å c=5.2054(2) Å for ZnO (Sowa & Ahsbahs 2006).

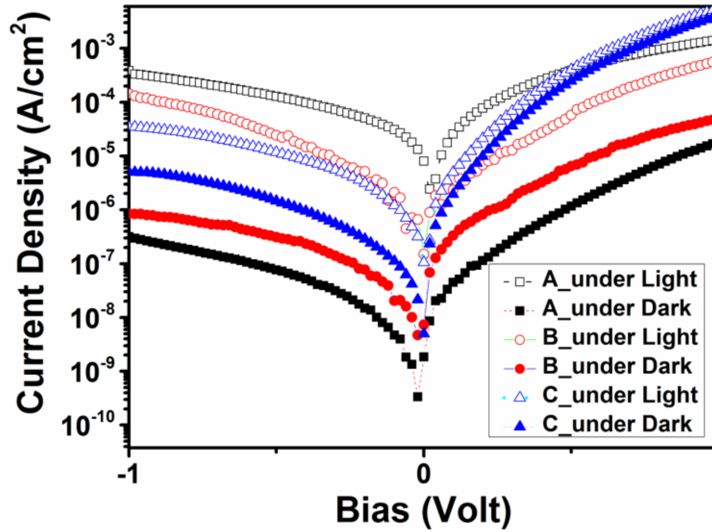

Figure 2.6: Current density versus voltage curve for Devices A, B, and C under dark condition and illumination of white LED (see the Appendix for the spectrum of the LED).

2.3.2 Device Characterization

The current density-voltage (J-V) relationships of device A, B, and C measured using the Agilent B1500A semiconductor parameter analyzer (SPA) from -1 to 1 V are shown in Figure 2.6. The J-V relationship of the device measured under dark and under the illumination of a white LED light with 96.8 μW/cm^2 intensity at 500 nm. The fabricated device behaves as the Schottky photodiode with a ZnO QDs and MoO_x as the charge transport layers. The active layer of the device is constituted by the CdSe QDs deposited over the ZnO QDs. The thermally grown MoO_x of ~8 nm forms a Schottky junction with the CdSe QDs (Litzov & Brabec 2013). ITO and Ag are used as a back and top electrode respectively. Further, the Schottky photodiodes are illuminated by a white LED source (96.8 μW/cm^2 at 500 nm) from the back side of the device to achieve 100% illumination area. Figure 2.6 indicates the edge of device A among the other

compared devices with the maximum photoresponse and minimum dark current. Device A shows the best contrast ratio of 1216 at an applied bias of -1 V as compared to 170.8 and 7 for devices B and C, respectively also indicated in Figure 2.6. The contrast ratio is defined as the ratio of the photocurrent to the dark current of a PD. The contrast ratio thus provides the information regarding the change in device current under illumination with respect to the dark current. It is calculated using photocurrent to dark current ratio $I_{ph}(V)/I_{dark}(V)$ measured at any fixed bias V.

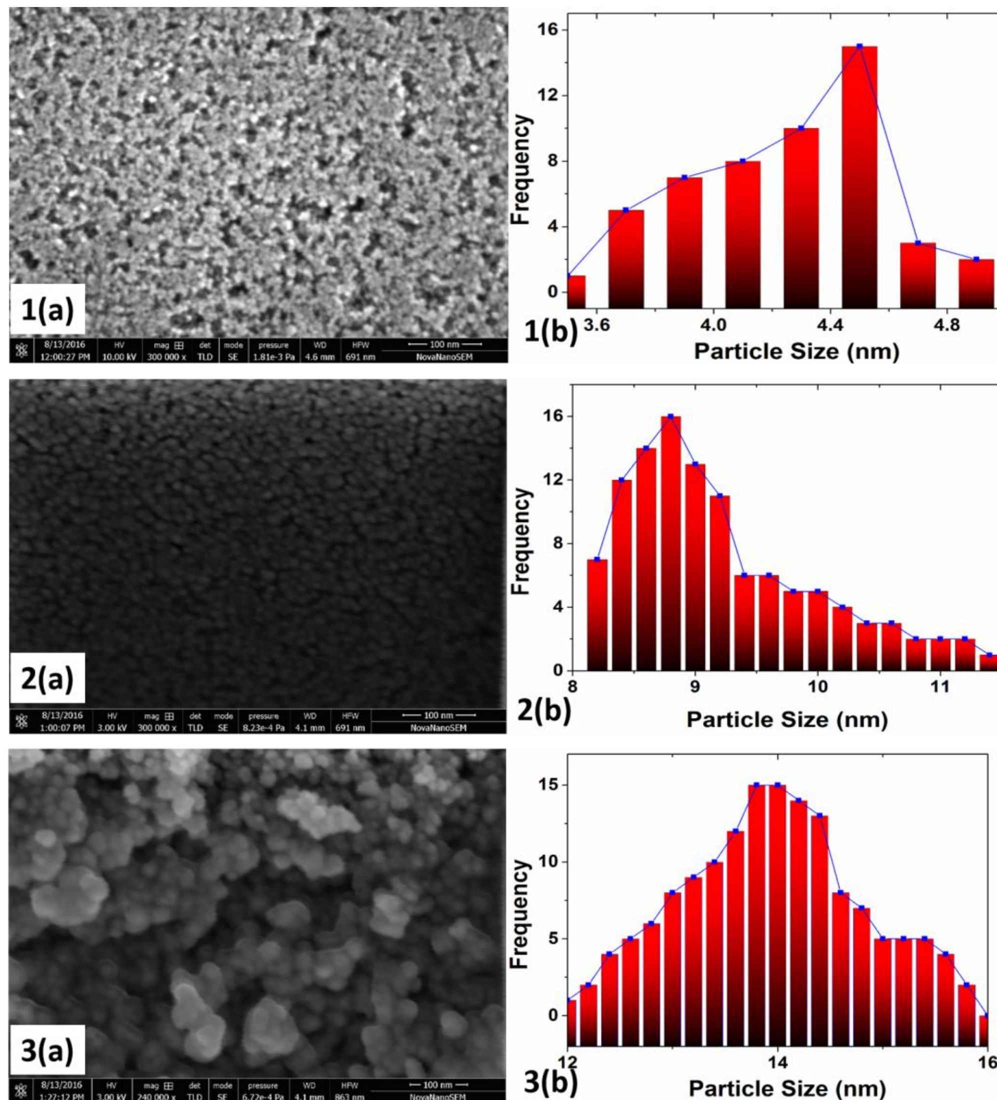

Figure 2.7: ZnO QDs HRSEM at a scale of 100 nm and particle size histogram for annealing temperatures at (1) 250°C, (2) 350°C, and (3) 450°C.

Device A also exhibits the lowest dark current (-0.02 μA) compared to device B (-0.06 μA) and C (-0.37 μA) at an applied bias of -1 volt. This result indicates the effect of annealing on the device performance. As the annealing temperature of the ZnO QDs is increasing, there is an increment in dark current. Hence, the device A having very low dark current shows better photoresponse and sensitivity compared to device B and C. The comparison of electrical properties such as reverse saturation current, barrier height and ideality factor of Device A, B and C are given in the Appendix. The variable results shown by the PDs are based upon the annealing effects of ZnO QDs; so it is necessary to analyze the thin film characteristics of ZnO QDs annealed at different temperatures.

Characterization of ZnO Thin Films: The surface morphology of ZnO QDs thin film annealed at 250°C, 350°C, and 450°C are shown in Figure 2.7. The calculated grain sizes of ZnO QDs annealed at 250°C, 350°C, and 450°C are ~4.42 nm, 8.74 nm and 13.89 nm with standard deviations of 0.41 nm, 1.49 nm, and 1.23 nm, respectively. The increase in annealing temperature enhances the merging of small QDs to form larger particle sized QDs which, in turn, largely affect the electrical and optical properties of the QDs (Drndić et al. 2002; Klimov 2010). For the case of direct bandgap semiconductor (e.g., ZnO), the maximum and minimum of the valence and conduction bands occur at *k=0.* The discrete energy levels in the valence band (E_k^v) and conduction band (E_k^c) can be approximated with the help of effective mass approximation as (Klimov 2010):

$$E_k^c = \frac{\hbar k^2}{2m_{eff}^v} + E_g \tag{2.1}$$

$$E_k^v = -\frac{\hbar k^2}{2m_{eff}^v} \tag{2.2}$$

$$k = \frac{\alpha_{n,l}}{a} \tag{2.3}$$

where $\alpha_{n,l}$ is the nth zero of Bessel function, a is the radius of the QDs and, E_g is the forbidden band gap between the conduction and valence bands defined as:

$$E_g = \frac{\hbar \alpha_{n,l}^2}{2a^2 m_{eff}^v} + E_{g,0} \tag{2.4}$$

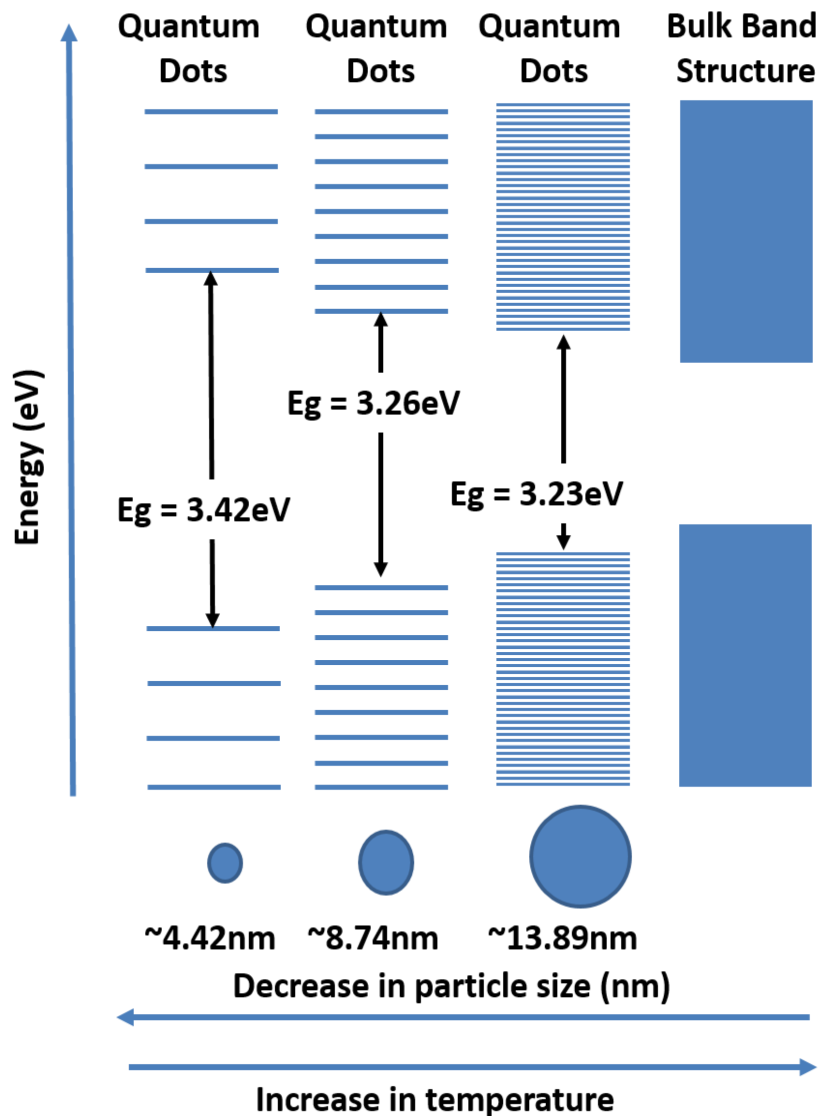

Figure 2.8: Band energy diagram of ZnO QDs against the particle size of ZnO QDs; increase in the particle size leads the discrete bands of ZnO QDs to continuum state.

where $E_{g,0}$ is the energy of state at $k=0$ and Equation 2.4 clearly indicates the effect of particle size on the forbidden energy band gap ($Eg \propto 1/a^2$). The particle size of QDs also defines the confinement effect on the charge carriers of QDs (Klimov 2010). With the decrease in the size of QDs, quantum confinement is increased thereby leading to the quantization of the energy bands as shown in Figure 2.8.

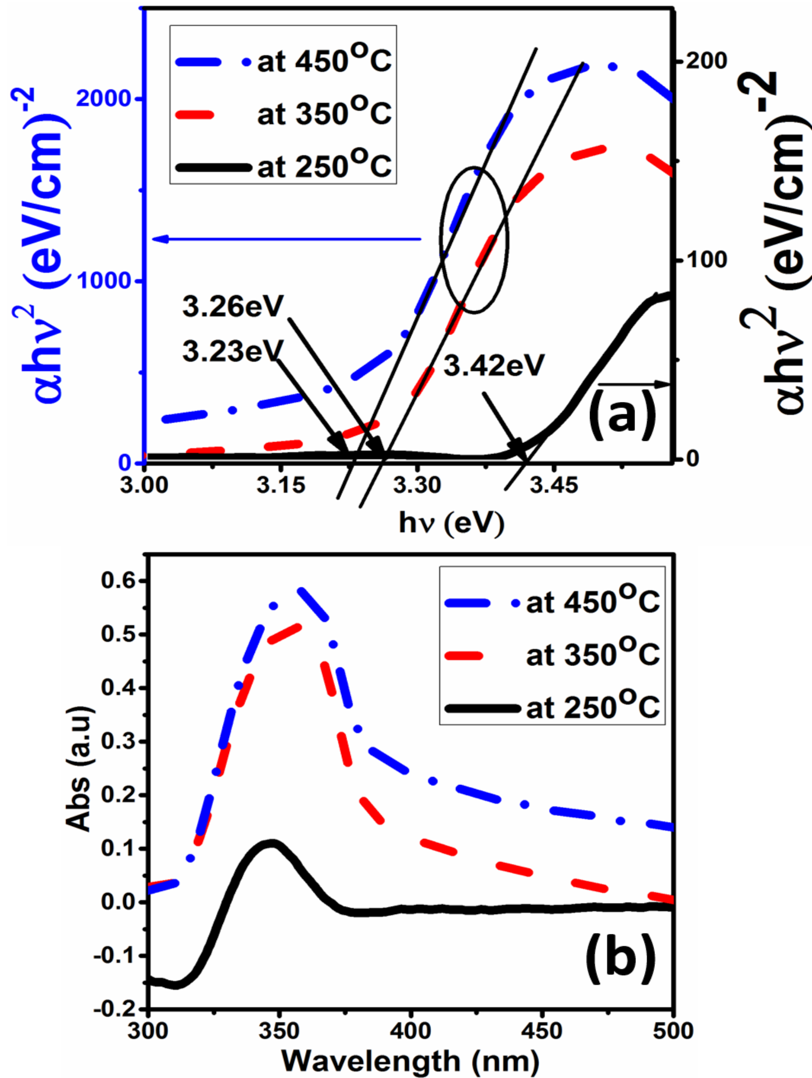

Figure 2.9: Optical study of ZnO QD film annealed at 250, 350, and 450 °C for (a) $\alpha h\upsilon^2$ versus hυ for bandgap calculation and (b) absorption curve of ZnO QD film.

This theoretical model is analyzed for the band-gap of ZnO QDs annealed at 250°C, 350°C, and 450°C. A shift in the absorption spectrum and the bandgap of the ZnO QDs

is observed with the increase in the annealing temperature as shown in Figure 2.9 (a) & (b). The ZnO QDs annealed at 250°C possess the maximum bandgap of ~3.42 eV, while the bandgaps of ZnO QDs annealed at 350°C and 450°C are 3.26 eV and 3.23 eV, respectively. Thus the annealing temperature results in the change in the absorption characteristics owing to bandgap changes as shown in Figure 2.9 (b). The absorption of the QDs keeps on increasing with the increase in annealing temperature shown in Figure 2.9 (b) and also in a trade with the previous study reported by *Drndic et al.* (Drndić et al. 2002) for CdSe QDs.

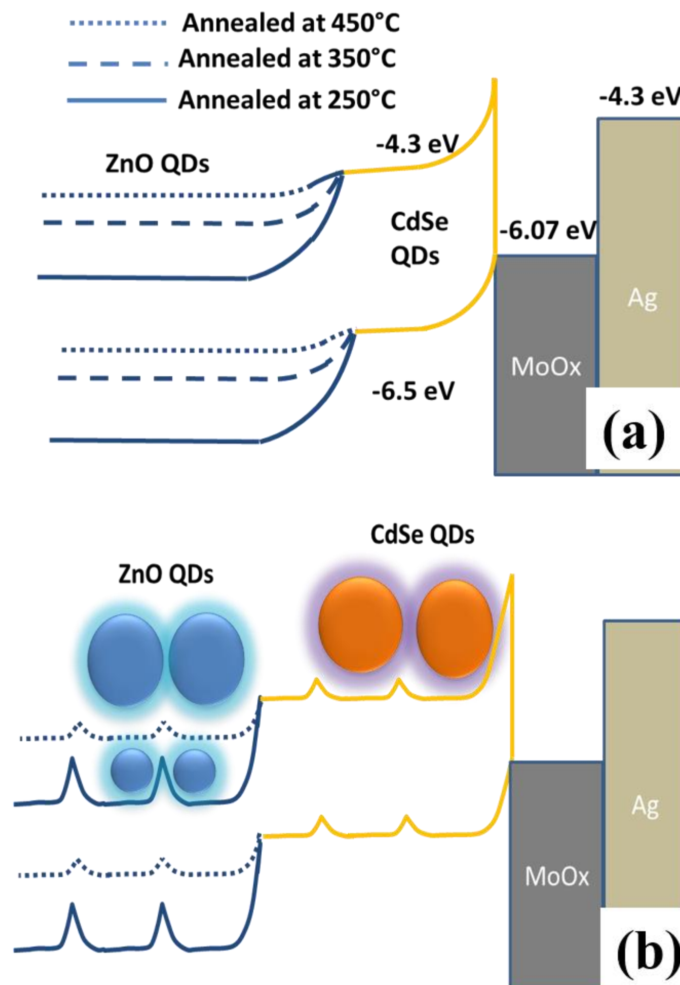

Figure 2.10: Band alignment diagram of Ag/MoO_x /CdSe QDs/ZnO QDs (a) for the different annealing temperatures (250, 350, and 450 °C) of ZnO QDs and (b) barrier between the two CdSe QDs and ZnO QDs; the barrier is dependent upon the size of the QDs.

Time Response Characteristics of PDs: The effect of ZnO QDs particle size on the electrical properties of the PDs can be explained by the band alignment diagram of the Ag/MoO_x/CdSe QDs/ZnO QDs as shown in Figure 2.10 (a). The electron affinity of ZnO QDs used is ~4.36 eV (Liu & Kelly 2013; Yang et al. 2015; Qian et al. 2011) while the ionization potential is measured using direct band gap of ZnO QDs measured in Figure 2.9 (a). The valence band energy levels of CdSe QDs is aligned with MoO_x which is suitable for the transportation of holes. However, the MoO_x provides a very high barrier for electrons generated in the active layer (CdSe QDs). The bandgap of ZnO QDs annealed at different temperatures provides variable barrier potential for the transportation of charge carriers. The barrier faced by the holes generated in active layer varies with the variation of annealing temperature of the ETL (ZnO QDs). The ZnO QDs provide the maximum barrier to the holes is ~1.26 eV when the ETL is annealed at 250°C which reduces to 1.1 eV at 350°C and 1.07 eV at 450°C annealing temperatures. This explains the variation of the photocurrent obtained in Figure 2.6 and explains the high photocurrent obtained with device “A” having an ETL of ZnO QDs annealed at 250°C. Furthermore, the QDs (ZnO and CdSe) separation also leads to a barrier in-between the consecutive QDs as shown in Figure 2.10 (b). The QDs have high surface potential, and it increases with the decrement of particle size, due to this high surface potential oxygen molecules adsorb the free electron $(O_2 + e^- \rightarrow O_2^-)$ in the surface and get ionized. This removal of electron from the surface depletes the surface of QDs from the charge carriers and results into the barrier between two consecutive QDs (Türe et al. 1987; Xu et al. 2014). These small barriers will behave like the small back to back Schottky barriers which depends upon the quantum confinement of the QDs (*w.r.t* particle size). The electron transfer between ZnO QDs using Marcus theory with necessary approximation has already discussed in chapter 1 sub-section 1.2.3.

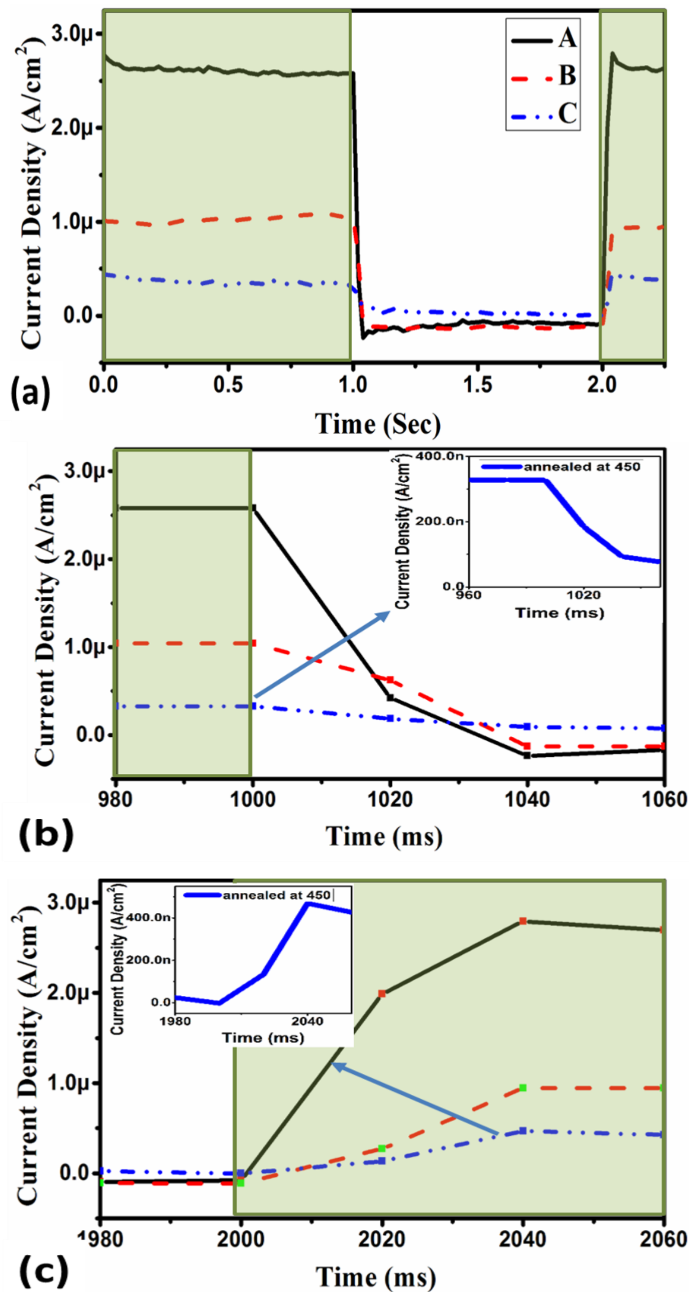

Figure 2.11: (a) Transient response of devices A, B, and C under illumination of white LED for 1 s at an applied bias of 0V, (b) Enlarged fall time responses of devices A, B, and C under zero bias, and (c) Enlarged rise time characteristics of devices A, B, and C under zero bias.

In contrast to the above discussion, the ZnO QDs annealed at 250°C exhibit greater Schottky barrier between the QDs compared to those of the ZnO QDs annealed at 350°C and 450°C. Further, the larger particles help in the flow of charges across the electrodes faster compared to smaller sized QDs under the dark condition also shown in

Figure 1.4 (b) and in a trade with Figure 2.6. The Schottky barriers across the QDs also affect the time-response characteristics of the devices. The time response characteristics of the fabricated devices are measured under the pulses (of period 1 sec) of white LED light (96.8 μW/cm^2 at 500 nm) illuminated from the back side of the devices. The result is plotted between the time (sec) and the photocurrent density (A/cm^2) measured using the digital multimeter (Agilent, 34410A) is shown in Figure 2.11 with the enlarged fall time and rise time characteristic shown in Figure 2.11 (b) & (c), respectively. The pulsating LED light source is obtained using Arduino™ microcontroller, and the digital multimeter is controlled by LabView™. The device "A" exhibits faster, and superior recovery response as compared to the devices B and C due to the effect of higher Schottky barriers in-between the ZnO QDs annealed at 250°C as shown in Figure 2.11. The fall time of device A dominates the recovery response with a fall time of 24.6 ms compared to 31.1 ms and 89.05 ms of device B and C respectively. Further, the rise time of device C shows fastest response of 23.13 ms compared to 26.4 ms and 32.3 ms of device A and B, respectively. The lowest average response time (i.e. highest average response speed) among the device A, B and C are found to be 25.5 ms for device A. While, for device B and C the response time is found to be 31.7 ms and 56.31 ms, respectively.

Photoresponse Characterization of PDs: The photocurrent density characteristics ($J_{ph}(\lambda, V) = \frac{(I_{ph}(\lambda,V) - I_{dark}(\lambda,V))}{A}$ is the modified photocurrent density of the detector excluding detectors dark current at a bias voltage *V*) of device A, B, and C at an applied bias of -0.1 V with the optical power density ($P_{opt}(\lambda)$ of the monochromatic source measured using power meter (PM100D, Thorlabs)) is shown in Figure 2.12 (a).

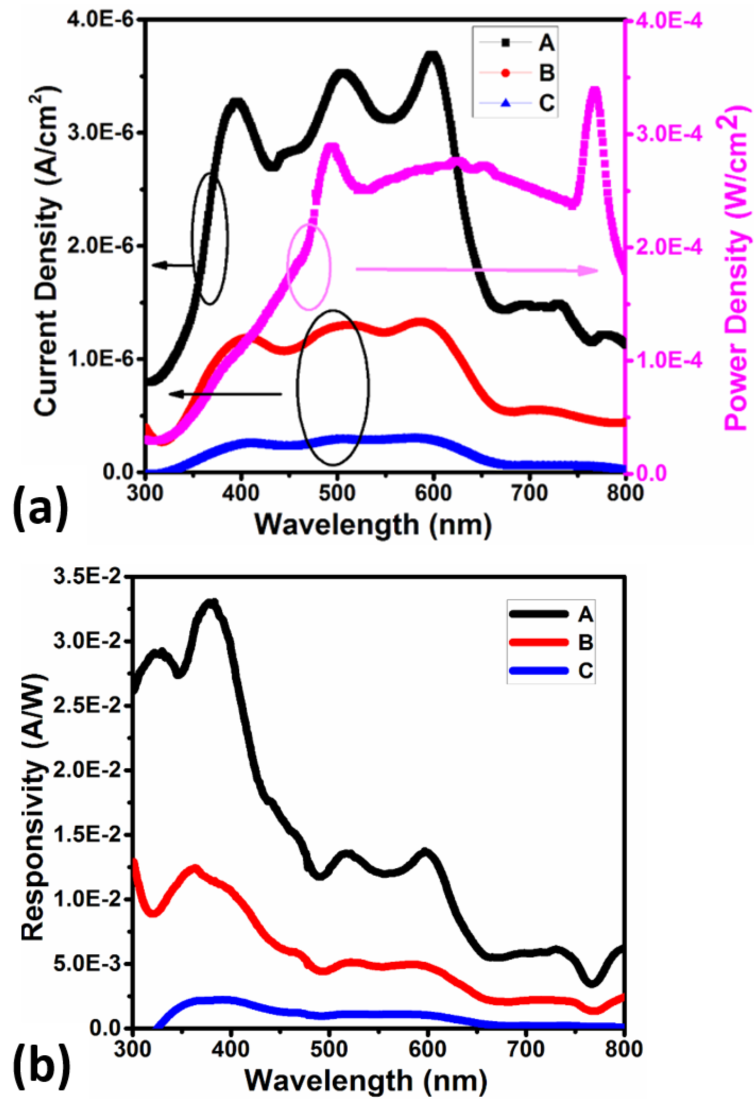

Figure 2.12: Devices A, B, and C are compared for (a) photocurrent with incident power density and (b) responsivity.

The device is illuminated from the back side to achieve the 100% illumination area using a monochromatic light produced by a monochromator (SP2150i) from Princeton Instruments. The photocurrent density plot in Figure 2.12 (a) indicates the enhanced response of device A over device B and C and shows the peak responses at ~400 nm, ~510 nm, and ~600 nm. The peak observed at ~400 nm is due to the filter effect of ZnO QDs used as an ETL in the devices.

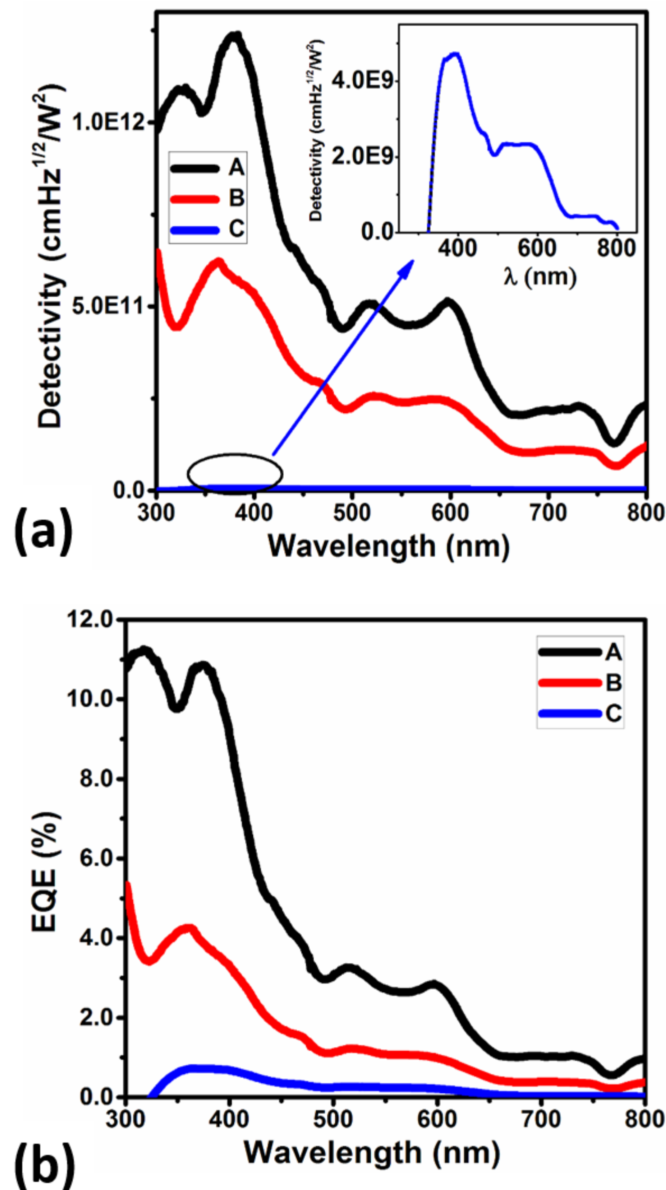

Figure 2.13: Devices A, B, and C are compared for (a) detectivity and (b) external quantum efficiency (EQE).

ZnO QDs absorbs short wavelengths (< ~390 nm) as shown in Figure 2.9 (b) and for a very small applied bias of -0.1 V ZnO QDs don't produce much photocurrent. Instead, effect of ZnO QDs particle size is evident on the photocurrent density plot over the UV region, ZnO QDs annealed at 250°C absorb very less UV light compared to ZnO QDs annealed at 350°C and 450°C which also signifies the results of ZnO QDs absorption curve shown in Figure 2.9 (b). The responsivity (*Re*), detectivity (*D**), and

external quantum efficiency (*EQE*) defines the quality of photodetector and can be calculated using following equations (Kumar et al. 2017):

$$R_e(\lambda) = \frac{J_{ph}(\lambda)}{P_{opt}(\lambda)} \tag{2.5}$$

$$D^*(\lambda, V) = R_e(\lambda, V) \times \left(\frac{RA(\lambda, V)}{4kT} \right)^{\frac{1}{2}} \tag{2.6}$$

$$EQE(\lambda, V) = \frac{1240 \times R_e(\lambda, V) \times 100}{\lambda} \tag{2.7}$$

where "*RA*" denotes the resistance–area product $RA(\lambda, V) = \left(\frac{dJ(\lambda, V)}{dV} \right)^{-1}$. The *Re*, *D** and *EQE* plot is shown in Figure 2.12 (b) and Figure 2.13 (a), & (b), respectively. Device A clearly shows the conceivably higher response compared to other two device B and C with the maximum responsivity, detectivity, and EQE of 0.03 A/W, 1.22×10^{12} $cmHz^{1/2}W^{-1}$, and 10.88%, respectively at a wavelength of 386 nm for an applied bias of -0.1 V compared to the maximum responsivity of 0.01 A/W and 0.002 A/W, maximum detectivity of 6.16×10^{11} $cmHz^{1/2}W^{-1}$ and 4.76×10^{9} $cmHz^{1/2}W^{-1}$, and maximum EQE of 4.25% and 0.76% of the other two PDs B and C.

2.3.3 Suitability of Annealed Colloidal ZnO QDs for Thin Film Transistors

We have observed that the electron transfer characteristics of the ZnO QDs vary with annealing temperature due to change in the particle size of the QDs. The size of ZnO QDs is observed to be increased with the annealing temperature. As a consequence, the ZnO QDs annealed at 250°C is found to be suitable for electron transport layer in photodiodes while it may not be suitable for other electronic applications. On the other hand, ZnO QDs annealed at 450°C is not suitable for the ETL

in the PDs but are good for the thin film transistors. In this section, we have briefly investigated the electrical performance of a Thin Film Transistor (TFT) using ZnO QDs annealed at 450°C.

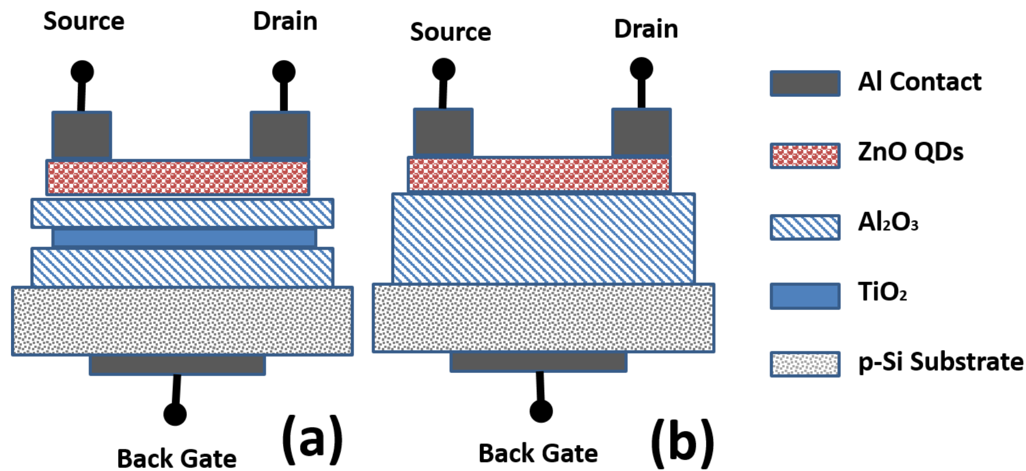

Figure 2.14: Schematic cross-sectional view of fabricated ZnO QDs based TFT (a) ZnO QDs based TFT with sandwiched TiO_2 layer between Al_2O_3 layers and (b) ZnO QDs based TFT without TiO_2 layer

The TFT structure is shown in Figure 2.14 (a) and (b) is fabricated on properly cleaned using p-Si substrates (2-7Ω-cm) by using standard cleaning procedure (RCA-1, RCA-2). The electron-beam evaporation (HHV, FL400 SMART COAT 3.0 A) is used for the deposition of Al_2O_3 (~ 8nm) as a tunnel oxide, TiO_2 (~10nm) as charge trapping layer, and Al_2O_3 (~12nm) as the blocking oxide in the form of A-T-A structure on the p-Si substrate. The prepared solution of the colloidal ZnO QDs (~ 100 nm) was deposited on the tunnel oxide A-layer by the spin coating method using SPM-150LC (TSE-system GmbH, Germany) spin-coater for fabricating two types of TFTs with and without a TiO_2 layer. The ZnO QDs are then annealed at 450ºC under ambient environment as discussed earlier. The top interdigitated ohmic contacts for source and drain are fabricated by depositing high purity Al (~50nm) by thermal evaporation on the ZnO QDs layer using interdigitated shadow mask technique while an Al layer of ~80nm

thickness is deposited on the entire back surface of the Si substrate for the Gate contact of the TFT.

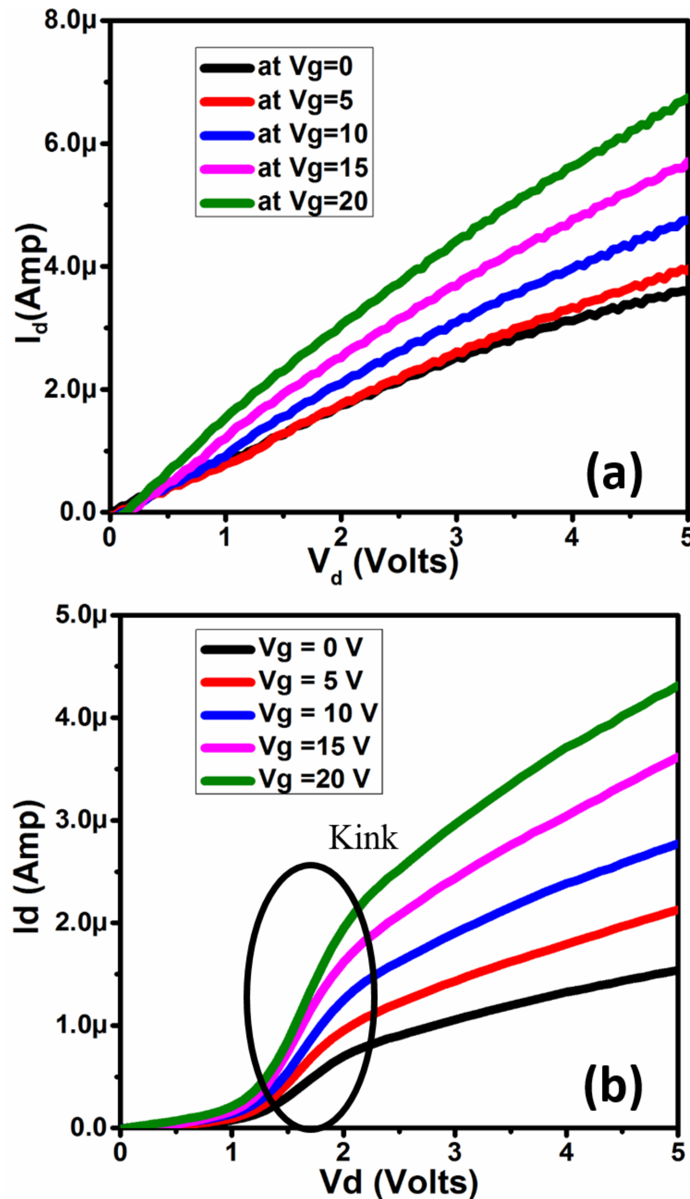

Figure 2.15: Drain current versus Drain voltage (a) for ZnO QDs based TFT without embedding floating gate of TiO_2 and (b) for ZnO QDs based TFT with embedding TiO_2 layer between the Al_2O_3 layers.

A very high vacuum (~10^{-6} bar) and a separation of ~18 cm between the source and substrate were maintained in the vacuum evaporation unit to achieve a growth rate of ~1.00 Å/s measured by the inbuilt digital thickness monitor (INFICON model no. SQM-160) attached to the coating unit. The measured drain current (I_{ds}) versus drain voltage

(V_{ds}) characteristics of the TFT with and without a TiO_2 layer have been shown in Figure 2.15 (a) and (b) respectively. The effect of TiO_2 in the ATA structure demonstrates the kink effect as shown in Figure 2.15 (b). The kink effect is the phenomenon caused by the injection of charges into the floating body (TiO_2) due to the effect of gate biasing. For the applied positive bias at the back gate, there will be a drift in charge carriers of ZnO QDs as the A-T-A layer act as a high-k material, and some of the negative charges (electrons) cross the barrier of Al_2O_3 and traps inside the floating body (TiO_2). Also, there will be an accumulation of holes at the interface of p-Si/Al_2O_3 and under the effect of the vertical electric field (at certain applied voltage), some of the holes tunnel through the tunnel oxide (Al_2O_3) and reach the floating body (TiO_2). These holes will liberate the trapped negative charges of TiO_2 leads to the current overshoot shown in Figure 2.15 (b).

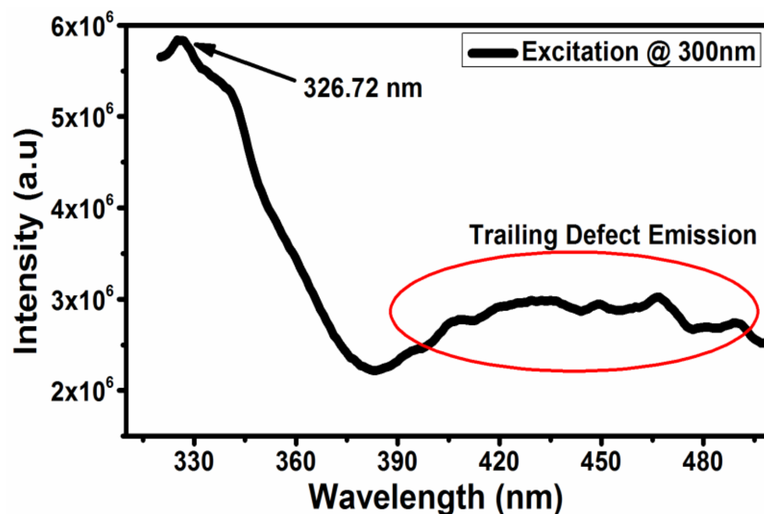

Figure 2.16: Photoluminescence of TiO_2 film.

The trapping of negative charge carriers also causes the reduction in the value of current (I_d) shown in Figure 2.15 (b) compared to the device without floating body (TiO_2) shown in Figure 2.15 (a). The charge trapped under the TiO_2 sandwiched by two

Al_2O_3 layers leads to the kink effect in the device. Surface defects in the TiO_2 layer are the most common charge trapping sites in the TiO_2 film. To understand the quality of the TiO_2 film, the photoluminescence (PL) is shown in Figure 2.16 with the excitation wavelength of 300 nm. The peak is obtained at 326.72 nm (~3.79 eV) while a trailing defect emission starting from 400 nm represents the surface defects which leads to the charge trapping sites on the surface of the TiO_2 film (Gfroerer 2006). Since the electron tunnelling across the Al_2O_3 layer occurs at low voltage, the kink effect in the transistor characteristics obtained by using a TiO_2 layer as floating body can be explored for designing the low power memory devices with further scaling at industrial grade (Inoh et al. 2003). This phenomenon can reduce the voltage of read/write operation thereby improving the efficiency of the memory devices.

2.4 Conclusion

The effects of heat treatment at 250°C, 350°C and 450°C of the colloidal ZnO QDs based ETL on the performance characteristics of ITO/ZnO QDs/CdSe QDs/MoO_x/Ag based PDs are analyzed for the first time. The colloidal CdSe QDs layer is used as the active layer, and MoO_x is used as the HTL in the PDs. The effect of annealing temperature on the particle size of ZnO QDs (i.e., ETL) and the response speed of the PDs have also been considered. The particle size of the ZnO QDs at 250°C, 350°C, 450°C annealing temperatures are observed as ~4.42 nm, 8.74 nm and 13.89 nm respectively. The increased particle size with the annealing temperature increases the absorption of the ZnO QDs layer and dark current of the PD under study. The PD with a lower particle size of ZnO QDs (~4.42 nm at 250°C temperature) show ~7.11 and ~173 times higher photoresponse than the PDs with ZnO QDs ETL of larger particle sizes of 8.74 nm at 350°C and 13.89nm at 450°C, respectively. Device with ZnO QDs annealed

at 250°C also shows higher response speed than the other two devices containing the ZnO QDs ETLs annealed at 350°C and 450°C. Further, the PD with ZnO QDs ETL annealed at 250°C shows the highest responsivity, detectivity and EQE of 0.03 A/W, 1.22×10^{12} $cmHz^{1/2}W^{-1}$, and 10.88%, respectively at a wavelength of 386 nm for an applied bias of -0.1 V. The ZnO QDs annealed at 250°C also enhances the extraction of generated charge pairs through ETL. The ZnO QDs ETL annealed at temperatures higher than 250°C increases the dark current and hence unsuitable for applications in PDs. However, such ZnO QDs annealed at high temperatures are suitable for other electronic devices. In order to demonstrate the suitability of the ZnO QDs annealed at high temperatures for other electronic devices, we have finally demonstrated the electrical characteristics of the TFTs using ZnO QDs (with size ~13.84 nm) annealed at 450°C to show a low-voltage Kink effect in the device characteristics.